



# Supramolecular Anchoring of Octahedral Molybdenum Clusters onto Graphene and Their Synergies in Photocatalytic Water Reduction

Marta Feliz, Pedro Atienzar, Maria Amela-Cortés, Noee Dumait, P. Lemoine, Yann Molard, Stéphane Cordier

## ► To cite this version:

Marta Feliz, Pedro Atienzar, Maria Amela-Cortés, Noee Dumait, P. Lemoine, et al.. Supramolecular Anchoring of Octahedral Molybdenum Clusters onto Graphene and Their Synergies in Photocatalytic Water Reduction. *Inorganic Chemistry*, 2019, 58 (22), pp.15443-15454. 10.1021/acs.inorgchem.9b02529 . hal-02364865

**HAL Id: hal-02364865**

**<https://univ-rennes.hal.science/hal-02364865>**

Submitted on 11 Dec 2019

**HAL** is a multi-disciplinary open access archive for the deposit and dissemination of scientific research documents, whether they are published or not. The documents may come from teaching and research institutions in France or abroad, or from public or private research centers.

L'archive ouverte pluridisciplinaire **HAL**, est destinée au dépôt et à la diffusion de documents scientifiques de niveau recherche, publiés ou non, émanant des établissements d'enseignement et de recherche français ou étrangers, des laboratoires publics ou privés.

# Supramolecular Anchoring of Octahedral Molybdenum Clusters onto Graphene and their Synergies in the Photocatalytic Water Reduction

*Marta Feliz,<sup>\*,†</sup> Pedro Atienzar,<sup>†</sup> Maria Amela-Cortés,<sup>‡</sup> Noée Dumait,<sup>‡</sup> Pierric Lemoine,<sup>‡</sup> Yann Molard,<sup>\*,‡</sup> and Stéphane Cordier.<sup>‡</sup>*

<sup>†</sup>Instituto de Tecnología Química (Universitat Politècnica de València – Consejo Superior de Investigaciones Científicas) Avd. de los Naranjos s/n, 46022 Valencia, Spain.

<sup>‡</sup>Université de Rennes, CNRS, ISCR - UMR 6226, ScanMAT – UMS 2001, F-35000 Rennes, France.

KEYWORDS. Metal cluster, graphene, photocatalysis, supramolecular chemistry.

ABSTRACT. Dihydrogen production from sunlight should become one of the most important energy production means in the future. To reach this goal, low-cost and efficient photocatalysts still need to be discovered. Here we show that red NIR luminescent metal cluster anions, once combined with pyrene containing cations, are able to photocatalytically produce molecular hydrogen from water. The pyrene moieties act simultaneously as energy transmitters and as

supramolecular linkers between the cluster anions and graphene. This association results in a hybrid material combining the emission abilities of pyrene and cluster moieties to the electronic conduction efficiency of graphene. Hydrogen evolution reaction (HER) studies show that this association induces a significant increase of H<sub>2</sub> production compared to that produced separately by clusters or graphene. Considering the versatility of the strategy described to design this photocatalytic hybrid material, transition metal clusters are promising candidates to develop new, environmentally friendly and low-cost photocatalysts for HER.

## INTRODUCTION

Transition metal clusters are molecular compounds that contain several metal atoms linked by metal-metal bonds.<sup>1</sup> With their exact and defined composition, they can be classified as intermediates between transition metal coordination complexes and metal nanoparticles. Their specificity, compared to coordination complexes, is the delocalization of electrons involved in the metal-metal bonds on the whole metallic architecture. As those are not confined on one metal center, transition metal clusters display intermediate behavior between atoms and bulk metals and, in particular show unique magnetic, optical or catalytic properties.<sup>2-10</sup> Yet, octahedral transition metal cluster compounds based on a Mo, W or Re scaffold (**Scheme 1a**) are particularly attractive to design functional hybrid nanomaterials with potential applications in optoelectronic,<sup>11-16</sup> lighting,<sup>17</sup> theranostic<sup>18-21</sup> or photocatalysis<sup>6-7, 9, 22</sup> applications. Because molybdenum or tungsten elements are cheap and abundant, cluster-based compounds constitute promising alternatives to costly Ir(III)-, Pt(II)- or rare earth – containing luminophores, or non-environmentally friendly lead hybrid perovskites, or cadmium containing quantum dots. They are synthesized as

$A_x[M_6X^i_8X^a_6]$  ternary alkali salts ( $A$  = alkali,  $x = 2 - 4$ ;  $X^i$  = inner ligand, usually halogen or chalcogen atoms;  $X^a$  = apical halogen ligand) using solid state chemistry techniques. Resulting powders or crystals behave like ceramics. That is probably the reason why, despite their outstanding functionalities, their use and studies were circumvented to a small community of scientists who, only around twenty years ago, opened the Pandora's box of their integration in functional materials and nanocomposites<sup>23-24</sup> *via* solution chemistry. Since, octahedral transition metal clusters form an integral part of nanoscience and were integrated in functional hybrid materials by various approaches either by direct integration, or after apical ligand exchange, cationic metathesis or host-guest complexation.<sup>25-28</sup> Among the metal cluster units, the  $[M_6I_8(\text{perfluoroalkylate})^a_6]^{2-}$  and  $[M_6I_8(\text{perfluorobenzoate})^a_6]^{2-}$  ( $M = \text{Mo or W}$ ) cluster anions are the most emissive, with emission properties depending on the pKa of the carboxylic acids.<sup>29-36</sup> Recently, they were used to develop theranostic tools,<sup>37</sup> lighting devices<sup>17</sup> or oxygen sensors,<sup>38</sup> but surprisingly, their catalytic abilities have been scarcely explored so far. Yet, their excellent abilities to emit light combined to their isotropic architecture, *i.e.* the presence of six metal atoms arranged orthogonally, that could all play the role of catalytic centers, prefigure good opportunities in photocatalysis for this family of compounds. In this work, we investigate the photocatalytic abilities of  $[Mo_6I_8(OCOC_2F_5)^a_6]^{2-}$  anion,<sup>33</sup> in one of the most emblematic reaction in the field of renewable energy: the production of hydrogen by water splitting using sunlight.<sup>39-42</sup> In this field, it is still very challenging to develop low-cost, but efficient enough, photocatalysts that can be further scaled up for industrial applications.<sup>39, 42-52</sup> Currently, most researches are directed toward the use of earth abundant transition metal materials and hybrid systems supported onto graphene.<sup>42, 53-58</sup> The potential of transition metal complex-based photocatalysts to replace conventional inorganic materials was recently reported.<sup>59</sup> Still, many challenges should be faced before

graphene-metal clusters nanocomposites become photocatalysts to address environmental and energy-related issues, for instance in terms of photostability and activity.<sup>60-61</sup> In fact, it is well known that graphene, because of its zero band gap semiconducting properties due to its extended conjugated system, possesses a high conductivity and electron mobility that favor charge separation and electron transport. Therefore, supporting photocatalysts onto graphene usually prevents the direct recombination of the hole–electron pair formed during light excitation and, as a result, facilitates the photogenerated electron transfer leading to an enhanced H<sub>2</sub> photocatalytic performance compared to neat photocatalysts. Hence, several photocatalysts, such as TiO<sub>2</sub> nanoparticles, CdQ (Q = S, Se) quantum dots, MoS<sub>2</sub> or more recently metal clusters, were supported onto graphene oxide (GO) or reduced graphene oxide (RGO).<sup>42, 62-66</sup>

Here we report on the synthesis, characterization and photophysical properties of bright red NIR emitting octahedral molybdenum cluster complexes bearing functional organic counter cations able to form a supramolecular adduct with graphene. Properties of the most promising candidate in terms of surface coverage were further investigated, in particular the photocatalytic efficiency in the hydrogen evolution reaction (HER) from water.

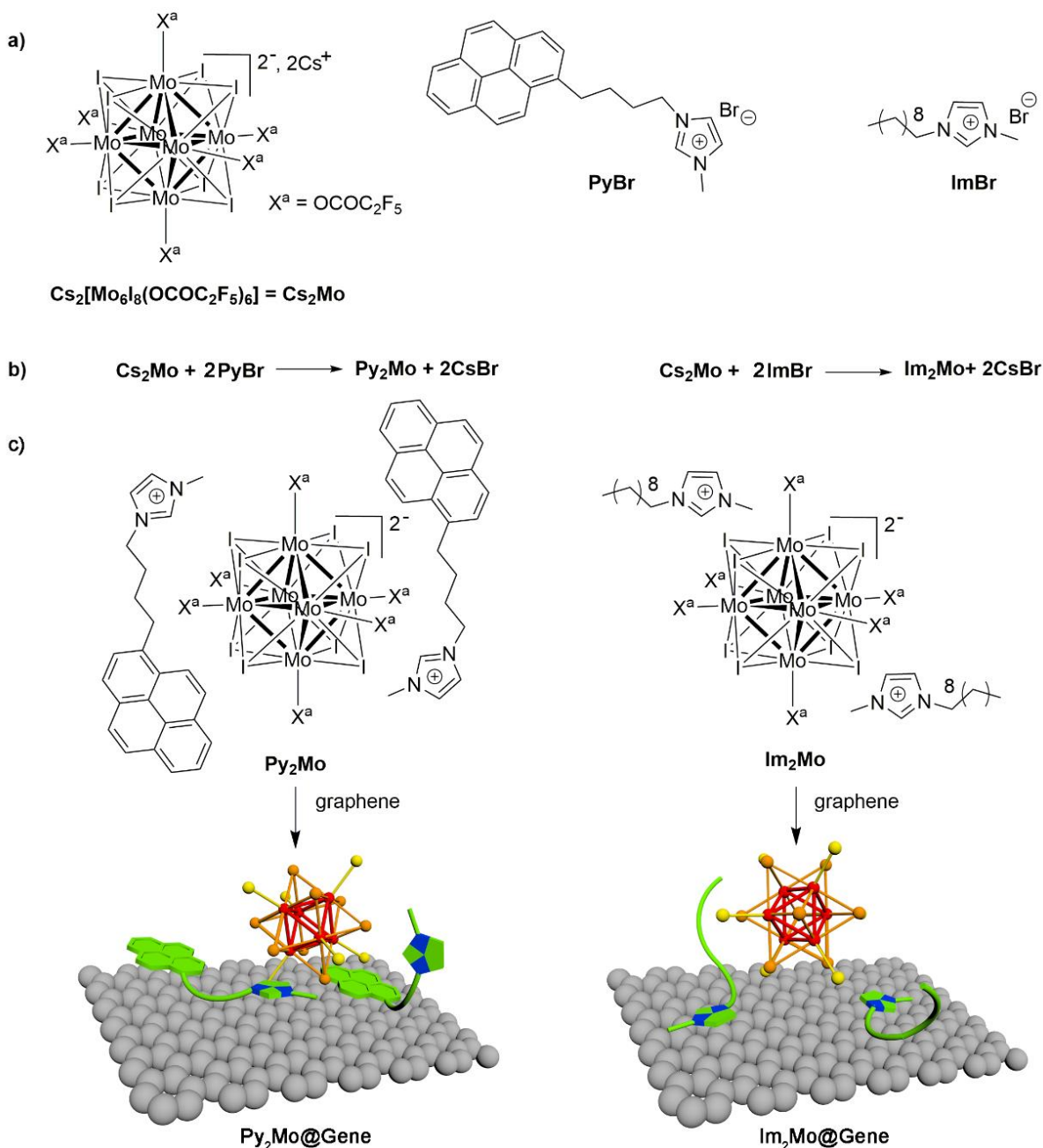
## RESULTS AND DISCUSSION

**Designing the linker for the anchoring of transition metal cluster on the graphene sheet: the supramolecular way.** It is now recognized that  $[M_6X_8X^a_6]^{2-}$  emission properties are related to the pK<sub>a</sub> value of their apical ligands, and that the most efficient emitters possess apical ligands linked to metal atoms via an acetate function.<sup>30, 34, 36</sup> Hence, the integrity of the  $[Mo_6I_8(OCOC_2F_5)^a_6]^{2-}$  anion should be preserved within the photocatalytic system to preserve its outstanding ability to emit light. In earlier studies, we observed that the covalent grafting of metal clusters on the surface of GO sheets limited the accessibility on the cluster active sites for catalytic

reactions.<sup>9</sup> Moreover, the graphene covalent functionalization alters the  $sp^2$  structure of its lattice which results in defects and loss of electronic properties. Therefore, the apical ligand exchange approach that allows the covalent grafting of the polymetallic anion onto any type of surface<sup>67-69</sup> has to be discarded. The non-covalent functionalization of graphene preserves its outstanding structural and electronic properties along with the simultaneous deposition of new chemical groups on the surface, and leads to an enhanced dispersability and catalytic reactivity of the hybrid material. For these reasons, using non-covalent interactions to link both protagonists appears as the most profitable way to take advantage of their properties. In fact, non-covalent functionalization of graphene or graphene oxide has been extensively studied to bind fluorophores or functional organic or inorganic species onto their surface.<sup>65, 70-72</sup> This technic should lead to hybrid materials that combine the best of each individual component properties. Hence, using supramolecular interactions to maintain the cluster anion on the graphene surface seems the more appropriate method to maximize the cluster effect during catalytic reactions.

The adsorption of polycyclic aromatic hydrocarbons (PAHs) and ionic liquids based on imidazolium cations onto graphene nanosheets has been recently investigated.<sup>73-74</sup> In the case of pyrene, its affinity to graphene is dominated by  $\pi$ - $\pi$  interactions, whereas in the case of ionic liquids, these and other non-covalent interactions, such as  $C-H \cdots \pi$ ,  $N \cdots \pi$  or  $ion \cdots \pi$  interactions, take place in the adsorption of imidazolium cations and their associated counteranions on the graphene surface.<sup>74-75</sup> Recently, Coskun and co-workers have shown that bifunctional pyrene-imidazolium molecules can interact with reduced graphene oxide through  $\pi$ - $\pi$  and cation- $\pi$ -interactions simultaneously with ionic liquid solvent molecules.<sup>76</sup> In this context, as depicted in **Scheme 1a**, we decided to synthesize an imidazolium cation bearing a pyrene group, noted as **Py<sup>+</sup>** (1-methyl-3-(4-(pyren-1-yl)butyl)-1H-imidazol-3-ium), to counterpart the anionic charge of the

metal cluster unit. Photoactive cluster units bearing planar aromatic molecules can add light harvesting,<sup>77</sup> energy and charge transfer features to graphene. The N-methyl-imidazolium



**Scheme 1.** Schematic representation of cluster compound precursor and organic imidazolium salts synthesised for these studies (a) and the hybrids **Py<sub>2</sub>Mo** and **Im<sub>2</sub>Mo** that will be further grafted onto graphene surfaces (b).

functionalized pyrene counterions should play a dual role: (i) to act as antenna and promote energy transfer to the luminescent  $\{\text{Mo}_6\text{I}_8\}^{4+}$  cluster core, and (ii) to assist the cluster immobilization onto graphene surfaces by non-covalent interactions. To observe the benefit of the pyrene group on its functional ability to be adsorbed onto the graphene surface, we also functionalized the cluster anion with imidazolium cations bearing a long alkyl chain, noted as **Im**<sup>+</sup> (1-methyl-3-nonyl-1H-imidazol-3-ium).

### Synthesis and characterization of the **Py<sub>2</sub>Mo**, **Im<sub>2</sub>Mo**, and **Py<sub>2</sub>Mo@Gene** materials.

The cationic metathesis between the  $\text{Cs}_2[\text{Mo}_6\text{I}_8(\text{OCOC}_2\text{F}_5)_6]$  (**Cs<sub>2</sub>Mo**) compound and the **PyBr** or **ImBr** salts afford quantitatively the **Py<sub>2</sub>Mo** and **Im<sub>2</sub>Mo** complexes, respectively, as highlighted in Scheme 1b. The **Py<sub>2</sub>Mo** and **Im<sub>2</sub>Mo** cluster compounds were characterized by <sup>1</sup>H and <sup>19</sup>F NMR spectroscopy, and electrospray ionization mass spectrometry (ESI-MS) in order to confirm the complexes identity and purity (see Experimental Section and Supporting Information for characterization details). The structure of the **Py<sub>2</sub>Mo** complex was further confirmed by single-crystal X-ray diffraction on suitable crystals obtained by slow evaporation of a complex containing acetone:toluene (1:1) solution (see Supporting Information).

The adsorption capacities of **Py<sub>2</sub>Mo** and **Im<sub>2</sub>Mo** by non-covalent interactions onto the graphene surface, resulting in **Py<sub>2</sub>Mo@Gene** and **Im<sub>2</sub>Mo@Gene** hybrid nanomaterials respectively (**Scheme 1c**), were investigated. Corresponding adsorption densities ( $q_e$ ) and adsorption isotherms were also determined (**Figure S3**, Supporting Information). The maximum adsorption capacity observed for **Py<sub>2</sub>Mo** at equilibrium is 0.3827 mmol (**Py<sub>2</sub>Mo**)/g (graphene). Considering the surface area of graphene (474 m<sup>2</sup>/g), the calculated cluster density deposited onto graphene surface is 0.0008 mmol/m<sup>2</sup>. The maximum  $q_e$  determined for **Py<sub>2</sub>Mo** is lesser than that reported for pyrene,<sup>74</sup> which is probably due to the high steric hindrance of the hybrid complex and to the fact that two



pyrene moieties are surrounding one metal cluster unit. The adsorption isotherms for both complexes shows a linear fitting, in agreement with Langmuir isotherms, with *ca.* 15% increment of the adsorption capacities for **Py<sub>2</sub>Mo** vs **Im<sub>2</sub>Mo**. These results support the relevant role of pyrene in reinforcing the non-covalent cluster immobilization onto graphene surfaces despite its bulkiness compared to the **Im**<sup>+</sup> cation. Hence, as the pyrene containing cation is the one that provides the best surface coverage, only the hybrid cluster compound **Py<sub>2</sub>Mo** and its adduct with graphene were further investigated. **Py<sub>2</sub>Mo@Gene** was thus obtained by mixing **Py<sub>2</sub>Mo** and graphene in dichloromethane at room temperature. The solid nanomaterial was isolated by filtration and washed with dichloromethane and diethyl ether, followed by vacuum drying.

The morphology of the **Py<sub>2</sub>Mo@Gene** material was characterized by high resolution transmission electron microscopy (HR-TEM). HR-TEM analyses of the **Py<sub>2</sub>Mo@Gene** material shows a heterogeneous distribution of 2-3 nm molybdenum cluster aggregates onto a few layer graphene support (**Figure S4**). The  $\pi$ - $\pi$  and cation- $\pi$  interactions between the pyrene functionalized imidazolium cations and graphene allow the hybrid system to self-assemble strongly, and these interactions also lead to the entrapment of cluster molecules between graphene layers, resulting in the formation of a 3D network structure. In addition, the cluster anion- $\pi$  interactions are not discarded in the adsorptive interactions.<sup>75</sup> The energy-dispersive X-ray spectroscopy (EDS-STEM) analysis of the hybrid material confirms the presence of Mo, I and F atoms (**Figure S5**).

The **Py<sub>2</sub>Mo@Gene** nanomaterial was further characterized by FT-IR, Raman, and photophysical based techniques. The infrared spectra registered for the **Py<sub>2</sub>Mo@Gene**, **Py<sub>2</sub>Mo** and graphene materials (**Figure 1a**) shows that there is no shift of the **Py<sub>2</sub>Mo** and graphene peaks after the cluster immobilization. The infrared spectrum of the **Py<sub>2</sub>Mo@Gene** solid contains most of the characteristic peaks of the **Py<sub>2</sub>Mo** complex. The bands at 1580 and 1628 cm<sup>-1</sup> of the graphenic materials are assigned to the C=C vibrations of the sp<sup>2</sup> carbon atoms and H-O-H vibrations of adsorbed water molecules, respectively. The Raman spectra of **Py<sub>2</sub>Mo**, graphene and the hybrid nanomaterial have been acquired in the solid state upon 325 nm laser irradiation (**Figure**

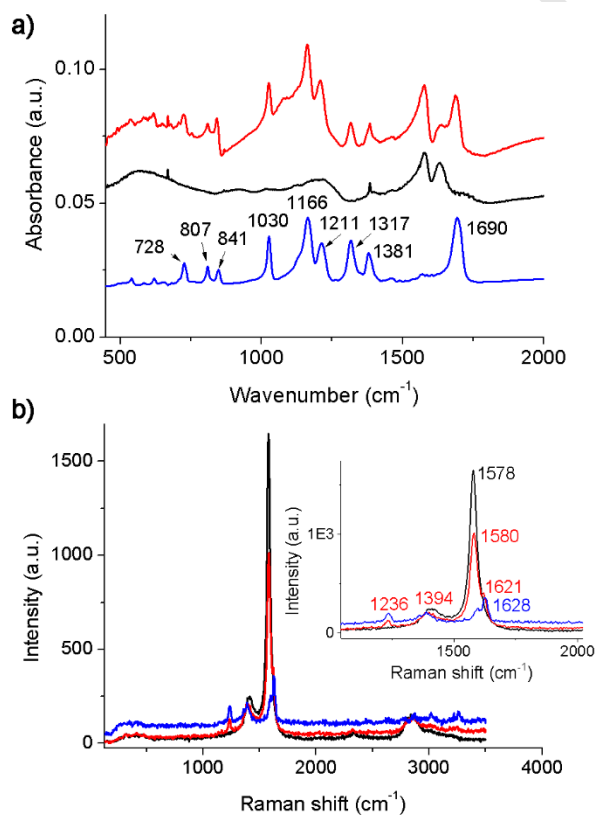


**Figure 1.** a) FT-IR (KBr) spectra of Py<sub>2</sub>Mo@Gene (red line), Py<sub>2</sub>Mo (blue line) and graphene (black line). The Py<sub>2</sub>Mo and graphene bands are highlighted; b) Raman spectra of Py<sub>2</sub>Mo@Gene (red line), Py<sub>2</sub>Mo (blue line) and graphene (black line). The inset shows the characteristic pyrene and graphene bands.

**1b).** The Raman bands between 150 and 500  $\text{cm}^{-1}$  expected for the  $\{\text{Mo}_6\text{X}_8\}^{4+}$  (X = halogen) cluster core complexes are not detectable, and only fluorescence has been obtained under 514 and 785 nm laser conditions.<sup>78-79</sup> The **Py<sub>2</sub>Mo@Gene** spectrum contains a very intense band at 1580  $\text{cm}^{-1}$  (G band) characteristic of the graphene aromatic rings  $\text{sp}^2$  carbon atoms vibration.<sup>80</sup> A wide band with a lower intensity appears at 1394  $\text{cm}^{-1}$  and includes a pyrene group Raman shift and the D band of graphene support. Two additional low intense bands characteristic of the pyrene functionality appear at 1236 and 1621  $\text{cm}^{-1}$ .<sup>81-82</sup> The graphenic 2D band (2848  $\text{cm}^{-1}$ ) does not show any displacement after the cluster immobilization.

#### **Photophysical properties of the Py<sub>2</sub>Mo and Py<sub>2</sub>Mo@Gene materials.**

Photophysical properties of **Py<sub>2</sub>Mo** were investigated in solution and compared to those of **PyBr** and **Cs<sub>2</sub>Mo** precursors. **Py<sub>2</sub>Mo** absorption spectrum shows the strongly pyrene absorbing bands centered at 325 nm (**Figure 2**) associated to the  $S_0 \rightarrow S_2$  transition, by analogy with similar systems.<sup>82-84</sup> The low absorption band intensity at 403 nm is associated to a metal to metal charge transfer (<sup>1</sup>MMCT) transition within the  $\{\text{Mo}_6\text{I}_8\}^{4+}$  cluster core.<sup>85-86</sup> This band is also observed in the **Cs<sub>2</sub>Mo** compound (**Figure S6**), which also shows absorption bands centered at 334 and 295 nm characteristic of the molybdenum to ligand cluster transitions. The appearance of these UV bands implies that there is a cluster contribution in the pyrene absorption region of the **Py<sub>2</sub>Mo** cluster compound (see **PyBr** absorption spectrum in **Figure S6** for comparison). The emission spectrum of **Py<sub>2</sub>Mo** in deaerated solution is presented in **Figure 2**. Upon excitation ( $\lambda_{\text{exc}} = 310 - 375 \text{ nm}$ ), two emission bands appear in the red and blue regions of the spectrum. The vibrational structure of the pyrene observed in the steady state fluorescence spectrum appears as a mirror image of the absorption spectrum. This fluorescence takes place from the  $S_1$  state, and is due to a

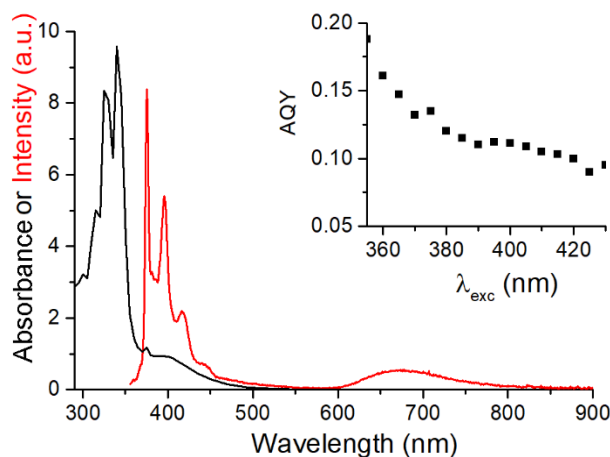


**Figure 2.** Absorption (black line) and emission (red line) spectra of  $\text{Py}_2\text{Mo}$  in deaerated solution ( $\lambda_{\text{exc}} = 345 \text{ nm}$ ) inset: absolute quantum yield vs excitation wavelength.

rapid internal conversion (IC) from the  $S_2$  to the  $S_1$  states upon excitation into the most intense pyrene absorption band centered at 345 nm.<sup>87</sup> Despite the presence of two pyrene units per  $\text{Py}_2\text{Mo}$ , the excimer emission from pyrene at *ca.* 500 nm is not observed. This highlights the lack of intra and intermolecular pyrene-pyrene interactions, taking in consideration the high dilution conditions ( $10^{-5}$  -  $10^{-6}$  M). A low intensity band with a maximum localized at 675 nm, attributed to the molybdenum cluster core emission, is also detected. This emission band shows a bathochromic shift with respect to the emission wavelength (650 nm) measured in DMF, also reported for  $\text{Cs}_2\text{Mo}$  in the solid state.<sup>33</sup> The disappearance of this band by bubbling  $\text{O}_2$  in the  $\text{Py}_2\text{Mo}$  containing solution confirms the oxygen-quenching of the cluster units phosphorescence. Absolute quantum yield (AQY) of  $\text{Py}_2\text{Mo}$  was measured exciting the sample every 5 nm from 355 up to 430 nm. The AQY decreases from 0.18 to 0.12 from 355 nm to 380 nm, *i.e.* when the pyrene emission is visible. This value stabilizes around 0.1 when the cluster is the only emitter. The  $\{\text{Mo}_6\text{I}_8\}^{4+}$  cluster core bearing perfluoroalkylcarboxylates presents one of the highest quantum yield value among the octahedral  $\{\text{M}_6\text{X}_8\}^{4+}$  ( $\text{M} = \text{Mo}, \text{W}$  or  $\text{Re}$ ;  $\text{L}^i = \text{halogen}$  or chalcogen) cluster complexes, and

quantum yields of 1 and 0.59 in solution were reported for  $(n\text{Bu}_4\text{N})_2[\text{Mo}_6\text{I}_8(\text{OOC}\text{CF}_3)_6]$  and  $(n\text{Bu}_4\text{N})_2[\text{Mo}_6\text{I}_8(\text{OOC}\text{C}_3\text{F}_7)_6]$ , respectively,<sup>30-31</sup> while we recently reported an AQY value of 0.49 in deaerated acetone for **Cs<sub>2</sub>Mo**.<sup>17</sup> Therefore, the **Py<sub>2</sub>Mo** AQY value is lower than the one calculated for its precursor **Cs<sub>2</sub>Mo**. In a first attempt, this observation can be explained as follow: the metal cluster red emission at 675 nm is subject to a partial energy transfer (ET) mechanism associated to intermolecular interactions between the pyrene and the molybdenum cluster. This ET is partly due to the spectral overlap between the emission band of the pyrene moiety and the absorption of the molybdenum cluster. A triplet-triplet state equilibrium between the triplet state of pyrene and the one of cluster could then be envisioned. This equilibrium would favor the non-radiative relaxation of the excited states (*vide infra*). **Figure 3** presents the evolution of the emission intensity maximum value of both entities, versus the excitation wavelength from 310 nm up to 390 nm, and the excitation map for excitations ranging from 355 up to 500 nm. The optimal wavelength to observe the pyrene emission is, as expected, around its maximum of absorption. Meanwhile, a band followed by a slight intensity decrease can be observed between 340 and 360 nm for the molybdenum cluster, in agreement with the maximum absorption of the pyrene group. This disrupt in the emission evolution trend is followed by an increase when the cluster is the only species to absorb (see **Figure S7** for the corresponding emission spectra). Then, the cluster emission slowly decreases due to its absorption lowering up to 500 nm. To assess in a first attempt that an effective transfer exists between the pyrene moieties and the anionic cluster unit, emission spectra of solutions containing **Py<sub>2</sub>Mo** or **Cs<sub>2</sub>Mo** at the same concentration, were recorded upon a 345 nm excitation. The increase of the cluster emission intensity by approximately 30%, is in good accordance with the pyrene-to-molybdenum cluster ET (**Figure S8**). The presence of pyrene

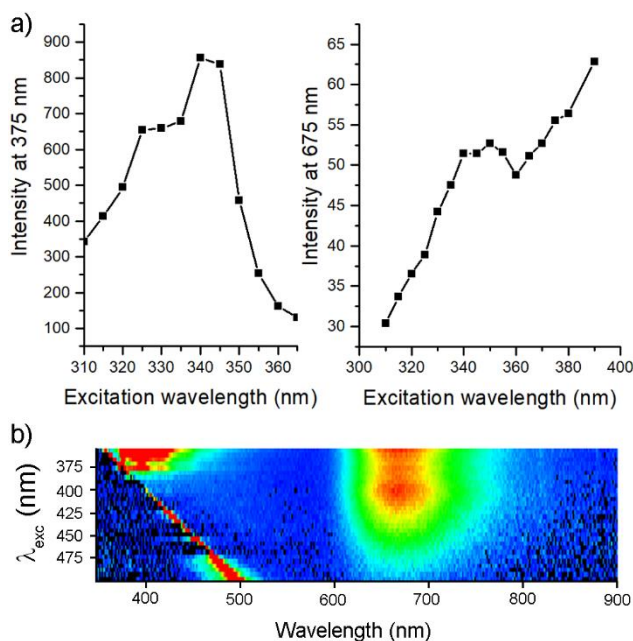


**Figure 3.** a) Evolution of Py<sub>2</sub>Mo emission maxima at 375 nm and 675 nm upon excitation; b) Emission vs excitation map of Py<sub>2</sub>Mo (emission intensity increases from dark blue to red).

emission signals indicates that the ET from the pyrene containing cation to the cluster core is not quantitative. Such non-quantitative ET were also recently evidenced in solution for assemblies gathering blue emissive triphenylene containing imidazolium cations and Red NIR emissive [Re<sub>6</sub>Se<sub>8</sub>CN<sub>6</sub>]<sup>4-</sup> anions.<sup>88</sup> It shows that, a short and covalent link between the pyrene and the cluster unit is mandatory to observe a full ET between the two entities and thus an enhancement of its emission efficiency.<sup>77</sup> We also monitored the emission signal of a solution containing initially **Cs<sub>2</sub>Mo** to which a small aliquot of a **PyBr** solution was added (see **Figure S9** for emission spectra). We observed an increase of the molybdenum cluster complex red emission in the presence of **PyBr**. The rise of the emission of **Cs<sub>2</sub>Mo** in the presence of **PyBr** is again in favor of a pyrene-to-cluster ET. To further characterize this partial ET, time dependent emission and absorption properties were investigated by time correlated luminescence spectroscopy and transient absorption (TA) spectroscopy.

Time resolved luminescence was also acquired at different excitation wavelengths. Emission lifetimes were extracted by fitting the experimental emission decay curves. The goodness of fits was judged looking at the  $\chi^2$  value and the shape of the residuals distribution. The phosphorescence lifetime for **Py<sub>2</sub>Mo** (188  $\mu$ s,  $\lambda_{\text{exc}} = 345$  nm in DMF) corresponds to the lifetime of the emissive {Mo<sub>6</sub>I<sub>8</sub>}-localized triplet states, and is similar to those reported for other carboxylate [Mo<sub>6</sub>I<sub>8</sub>(OOC-R)<sub>6</sub>]<sup>2-</sup> (R = CF<sub>3</sub>, 182  $\mu$ s; R = n-C<sub>3</sub>F<sub>7</sub>, 303  $\mu$ s) complexes in acetonitrile.<sup>30-31</sup> The higher emission lifetime of **Cs<sub>2</sub>Mo** (228  $\mu$ s,  $\lambda_{\text{exc}} = 345$  nm) suggests that the emission decay is faster for the **Py<sub>2</sub>Mo** complex, associated to any kind of counterion-cluster interaction.<sup>89</sup> This decrease in the lifetime and the slight bathochromic shift of the cluster emission maximum when Cs<sup>+</sup> is replaced by Py<sup>+</sup> could be due to an electronic stabilization of the cluster excited state by the pyrene-imidazolium counterion.<sup>90-92</sup> The decrease of the pyrene fluorescence lifetime from **PyBr** to **Py<sub>2</sub>Mo** (200 and 164 ns, respectively upon  $\lambda_{\text{exc}} = 340$  nm, see **Figure S10** for fluorescence decay profiles), confirms this partial interaction.

The transient absorption spectra of **PyBr** and **Py<sub>2</sub>Mo** compounds are presented **Figure 4a**. For **PyBr**, the spectrum shows the characteristic transient absorptions of the pyrene group triplet states of the functionalized imidazolium cation, which appear as two maxima centered at *ca.* 420 and 500 nm.<sup>93</sup> These triplet states are confirmed by quenching experiments with O<sub>2</sub> (**Figure S11**). At low absorption times a negative band corresponding to the emission of pyrene group singlet state (**Figures S12a** and **S12c**) appears between 350-450 nm. The **Py<sub>2</sub>Mo** and **Cs<sub>2</sub>Mo** TA spectra acquired upon 355 nm excitation are very similar and show a broad absorption band with one maximum centered at *ca.* 520 and 550 nm, respectively (**Figure S12** for **Cs<sub>2</sub>Mo** TA spectrum).

The temporal profiles acquired at 550 nm (**Figure S13**) show that the absorption lifetime of the triplet state for **Py<sub>2</sub>Mo** is faster than **Cs<sub>2</sub>Mo**, in agreement with the different lifetimes stated above.

Both absorptions are sensitive to O<sub>2</sub> indicating their triplet state nature, as previously shown by steady state luminescence experiments (**Figures S11b** and **S11d**).

The absorption temporal profiles measured for **PyBr** and **Py<sub>2</sub>Mo** indicate that the triplet pyrene group absorption at 420 nm involves a fast decay in the **Py<sub>2</sub>Mo** compound, in contrast to the profile measured for **PyBr** (**Figure 4b**). This result confirms the ET from the pyrene group of the imidazolium functionalized cation excited state to the molybdenum cluster anion. The deactivation of the pyrene group triplet state by the cluster core was confirmed by monitoring the decrease of the pyrene triplet state (420 nm) with sequential addition of small volumes of a stock solution of **Cs<sub>2</sub>Mo** to a solution of **PyBr** (see **Figure S15** for temporal profiles). We propose two possible reaction paths in the energy transfer mechanism within the **Py<sub>2</sub>Mo** complex, by taking energy

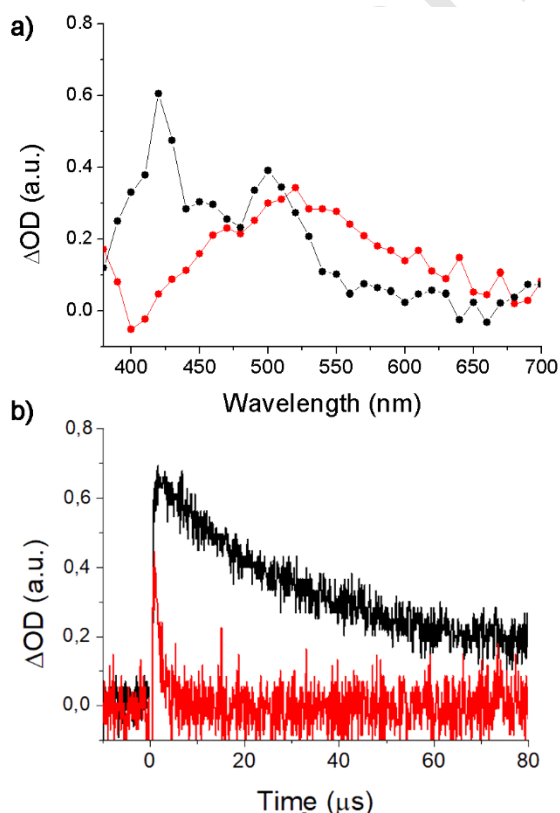
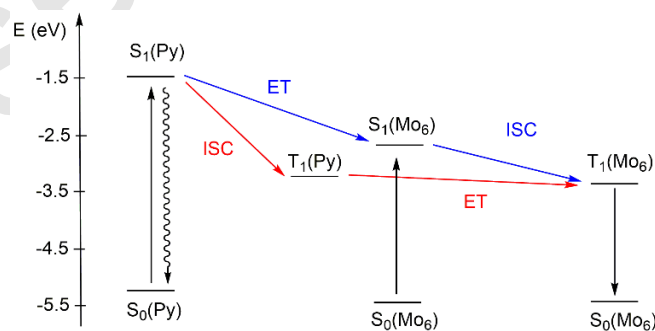


**Figure 4.** a) TAS (5μs after pulse) and b) temporal profiles of Py<sub>2</sub>Mo (red) and PyBr (black) acquired under argon in DMF.



positioning of cluster orbitals, calculated from the absorption and redox data of  $[\text{Mo}_6\text{I}_8(\text{OCOC}_2\text{F}_5)_6]^{2-}$  (see **Supporting Information**, section IV for details about calculations), and the pyrene orbitals.<sup>34, 94-96</sup> In both paths, the increase of the cluster unit phosphorescence at 675 nm could be attributed to a combination of an ET and intersystem crossing (ISC) processes ensuring that the energy migrates from the pyrene group and the  $\{\text{Mo}_6\text{I}_8\}^{4+}$  cluster core localized singlet excited states to the  $^3\text{MMCT}$  state of the cluster unit. Upon excitation in the UV region, regarding to the first mechanism proposed (blue line, **Scheme 2**), the pyrene group  $S_1$  excited state transfers the absorbed energy to the molybdenum cluster  $S_1$  excited state, and the remaining energy is lost by fluorescence relaxation. The  $S_1$  cluster state goes forward to an intersystem crossing (ISC) to the  $T_1$  of the  $\{\text{Mo}_6\text{I}_8\}^{4+}$  cluster core. In a second mechanism (red line, **Scheme 2**), the excited state of the pyrene group of the imidazolium functionalized counterion evolves to an ISC to its  $T_1$  triplet state, which transfers some energy to the emissive cluster-localized triplet state. We consider that the contribution of the reaction path referring to  $S_1(\text{Py})$  to  $T_1(\text{Py})$  ISC transition in the global mechanism is minor because of the low amount of pyrene group triplet state formed. Thus, the preferred path corresponds to the  $S_1(\text{Py})$  to  $S_1(\text{Mo}_6)$  ET transition, in agreement with



**Scheme 2.** Energy diagram of the possible reaction paths passed on the photophysical properties of **Py<sub>2</sub>Mo** (ET = energy transfer; ISC = Intersystem crossing). Energy scale relative to vacuum.

previous studies realized on the  $[\text{Mo}_6\text{I}_8(\text{OCO-pyrene})^a_6]^{2-}$  complex for which, an intramolecular ET takes place quantitatively.<sup>66</sup> Additionally, taking into account the energy positions of  $T_1(\text{Py})$  (-3.1 eV) and  $T_1(\text{Mo}_6)$  (-3.4 eV) as well as the low lifetime detected by TAS, a triplet-triplet equilibrium can be discarded. Therefore, the reaction path referring to  $S_1(\text{Py})$  to  $T_1(\text{Py})$  ISC transition can be considered as less probable because of the low amount of pyrene triplet state formation.

### **Interactions between $\text{Py}_2\text{Mo}$ and graphene in $\text{Py}_2\text{Mo@Gene}$ .**

The electronic interactions between  **$\text{Py}_2\text{Mo}$**  and graphene, were evidenced by steady state and time resolved photoluminescence spectroscopies. In the steady state regime, adding aliquots of a single- and few-layer thickness graphene suspension in DMF to a DMF solution containing the  **$\text{Py}_2\text{Mo}$**  complex ( $\lambda_{\text{exc}} = 375 \text{ nm}$ ) leads to a progressive decrease of the pyrene and  $\{\text{Mo}_6\text{I}_8\}^{4+}$  cluster core emission bands (see Figure S15a for emission spectra). This quenching of the  **$\text{Py}_2\text{Mo}$**  photoluminescence characterizes a non-radiative ET from  **$\text{Py}_2\text{Mo}$**  to the adjacent graphene surface, although the photoluminescence of graphene layers is negligible.<sup>97</sup> The time resolved luminescence spectra (**Figure S15b**) confirm the ET from the pyrene localized excited states to the  $\pi$  system of graphene, as the pyrene group lifetime decreases upon increasing the graphene concentration. The emission decay profiles could be fitted with a double exponential function, which indicates a dynamic quenching of the pyrene excited states. Two lifetime components appear for each decay curve: one in the scale of pyrene lifetime and a faster one associated to the presence of graphene. The relative ponderation of both components evolves upon addition of graphene. In fact, the weight of the pyrene component changes from 32% after addition of 125  $\mu\text{L}$  of graphene to 14% with 850  $\mu\text{L}$  of graphene suspension. These observations are also consistent with an ET from  **$\text{Py}_2\text{Mo}$**  to graphene.<sup>98</sup> Moreover, steady-state and lifetime fluorescence

quenching studies with graphene revealed deviation from linearity in the Stern-Volmer plots (**Figure S16**), indicating a collective effect of static and dynamic quenching. This could be explained considering the initial complex formation between the pyrene derivative compound and the graphene layers at the ground-state together with the collisional quenching of the remaining excited states of the pyrene units. The interaction between the **Py<sub>2</sub>Mo** complex and the graphene support in the **Py<sub>2</sub>Mo@Gene** nanomaterial was also studied by TAS. The absorption spectrum of the hybrid material (**Figure S17**) is dominated by a broad band absorption characteristic of graphene, which is attributed to the formation of delocalized electron and hole pairs along the nanostructure.<sup>99-100</sup> The TAS of the **Py<sub>2</sub>Mo@Gene** hybrid exhibits the pyrene emission band with maximum at 400 nm and a small absorption band at 540 nm assigned to the triplet state of the molybdenum cluster. The low intensity of the molybdenum band and the short lifetimes (**Figure 5**) associated to the temporal profiles of the **Py<sub>2</sub>Mo@Gene** material confirm the quenching of the excited state of molybdenum cluster by the graphene support, and suggests that any energy transfer takes place also from the cluster complex to the graphene support.<sup>98</sup> Therefore, this photoinduced charge transfer from the **Py<sub>2</sub>Mo** complex to the graphene layer produces a synergetic effect,

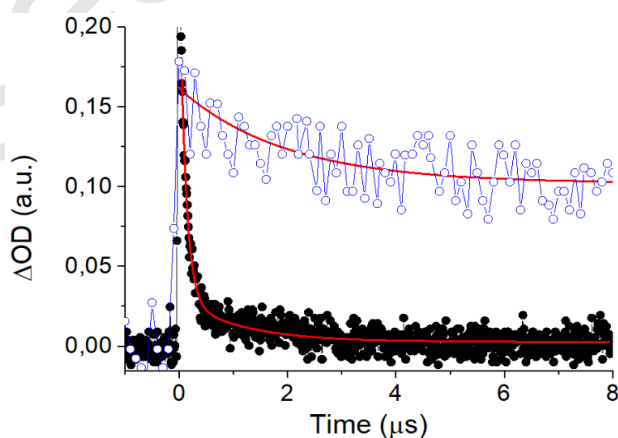


**Figure 5.** Absorption temporal profiles of **Py<sub>2</sub>Mo@Gene** (0.5 mg/mL, black line) and of **Py<sub>2</sub>Mo** (blue line) monitored at 580 nm after 355 nm laser excitation of a N<sub>2</sub> purged dichloromethane solution.

favoring the charge separation process after irradiation and enhancing the photocatalytic conversion as we describe below.

### Photocatalytic HER studies.

A comparative photocatalytic activity study of the **Py<sub>2</sub>Mo@Gene**, **Py<sub>2</sub>Mo** and graphene materials for molecular hydrogen generation from water was studied in a water:acetone (50:45% v/v) mixture in the presence of triethylamine (TEA, 5% v/v) under UV-Vis irradiation. Irradiations were carried out, with continuous stirring, using a cylindrical Pyrex reactor and a fiber optic Xe light source (800-200 nm emission output, 1000 W/m<sup>2</sup>). The evolution of photoreactions was monitored over time by means of gas chromatography. After 6 h of irradiation, dihydrogen was the only gas generated, and the performance of catalysts was evaluated in term of H<sub>2</sub> yield. The H<sub>2</sub> yields (μmol of H<sub>2</sub>·g<sub>cat</sub><sup>-1</sup>) with respect to time using the three photocatalysts are illustrated in **Figure 6**. The nanosized **Py<sub>2</sub>Mo@Gene** composite exhibits higher H<sub>2</sub> production in the

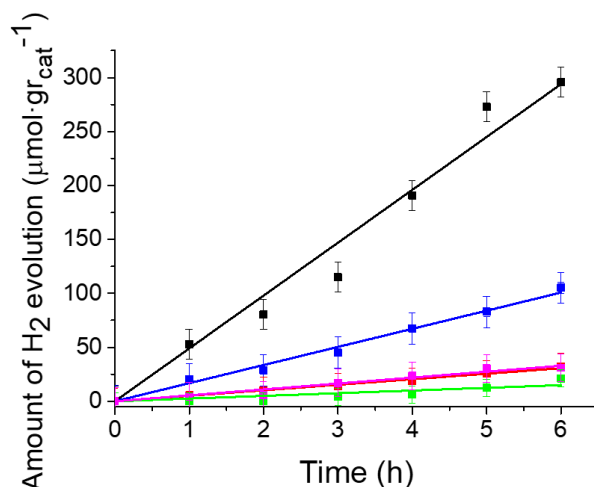


**Figure 6.** HER (μmol of H<sub>2</sub>·grcat<sup>-1</sup>) vs time plot by using Py<sub>2</sub>Mo@Gene (black line), Py<sub>2</sub>Mo (blue line), PyBr (green line) and PyBr-Gene (pink line) and graphene (red line) catalysts. Py<sub>2</sub>Mo, PyBr and PyBr-Gene used in equimolar amount as in Py<sub>2</sub>Mo@Gene.

photocatalytic reaction than the **Py<sub>2</sub>Mo** and graphene counterparts, resulting in an increase of the photocatalytic activities by 280%. After 6 h of irradiation, the hydrogen formation rate by using **Py<sub>2</sub>Mo@Gene**, **Py<sub>2</sub>Mo** and graphene catalysts was 49, 18, and 5  $\mu\text{mol of H}_2 \cdot \text{g}_{\text{cat}}^{-1} \cdot \text{h}^{-1}$ , respectively. The reaction rate of the hybrid nanomaterial is in the range of that reported for other MoS<sub>2</sub>/graphene catalytic systems in photochemical conditions (Table S2), although other complex systems are more efficient.<sup>101-104</sup> The catalytic activity of **Py<sub>2</sub>Mo@Gene** is comparable to that reported for some TiO<sub>2</sub>-, CdS- and C<sub>3</sub>N<sub>4</sub>/graphene nanomaterials in the absence of Pt as co-catalyst.

The small amount of hydrogen generated by neat graphene can be ascribed to the production of active catalytic species by ageing the graphene materials under photochemical conditions.<sup>105</sup> The turnover number (TON) calculated with respect to the **Py<sub>2</sub>Mo** cluster for **Py<sub>2</sub>Mo@Gene** and **Py<sub>2</sub>Mo** samples were found to be 0.96 and 0.34, respectively. The turnover frequency (TOF) with respect to atomic molybdenum for **Py<sub>2</sub>Mo@Gene** corresponds to  $7 \times 10^{-6} \text{ s}^{-1}$ . This is of the same order than the TOF values we observed for the (TBA)<sub>2</sub>Mo<sub>6</sub>Br<sub>8</sub><sup>i</sup>@GO composite for photocatalytic HER in similar conditions, whereas the TOF for **Py<sub>2</sub>Mo** ( $3 \times 10^{-6} \text{ h}^{-1}$ ) is two order of magnitude lower than that reported for the (TBA)<sub>2</sub>Mo<sub>6</sub>Br<sub>8</sub>F<sub>6</sub><sup>a</sup> complex.<sup>9</sup> The reaction rates for the **Py<sub>2</sub>Mo@Gene** nanomaterial and for the **Py<sub>2</sub>Mo** complex are nearly constant, and no induction period appears, in contrast to the (TBA)<sub>2</sub>Mo<sub>6</sub>Br<sub>8</sub>F<sub>6</sub><sup>a</sup> catalyst. This suggests that the integrity of the **Py<sub>2</sub>Mo** species is maintained under reaction conditions. After three reuse experiments of **Py<sub>2</sub>Mo@Gene**, the morphology of the nanomaterial remains intact (**Figure S18**), with 10% w/w molybdenum leaching after each experiment. Control experiments were carried out and show that **Im<sub>2</sub>Mo/Gene**, **Cs<sub>2</sub>Mo/Gene** and **PyBr/Gene** composites are less active than the **Py<sub>2</sub>Mo@Gene** hybrid, and that H<sub>2</sub> production is attributed to the molybdenum clusters (see **Figures 6** and **S24**).

We detect a slight increase of the activity of **Im<sub>2</sub>Mo/Gene** with respect to **Cs<sub>2</sub>Mo/Gene** (see **Figure S24**), which could be attributed to a better contact of **Im<sub>2</sub>Mo** to the graphene surface promoted by the imidazolium counterions.

These results confirm that **Py<sub>2</sub>Mo** acts as both photosensitizer and catalyst for hydrogen production under UV-Vis irradiation, similarly to the (TBA)<sub>2</sub>Mo<sub>6</sub>Br<sub>8</sub>F<sub>6</sub><sup>a</sup> photocatalyst. The enhancement of reaction yields provided by the graphene-supported cluster is due to the intimate contact between the **Py<sub>2</sub>Mo** catalyst and the graphene, and to the superior conductivity of graphene, since it acts as an efficient electron acceptor and transporter between the immobilized cluster active species (**Figure 7**). This is in agreement with reported works on dye-sensitized graphene-based photocatalysts.<sup>59, 106</sup>

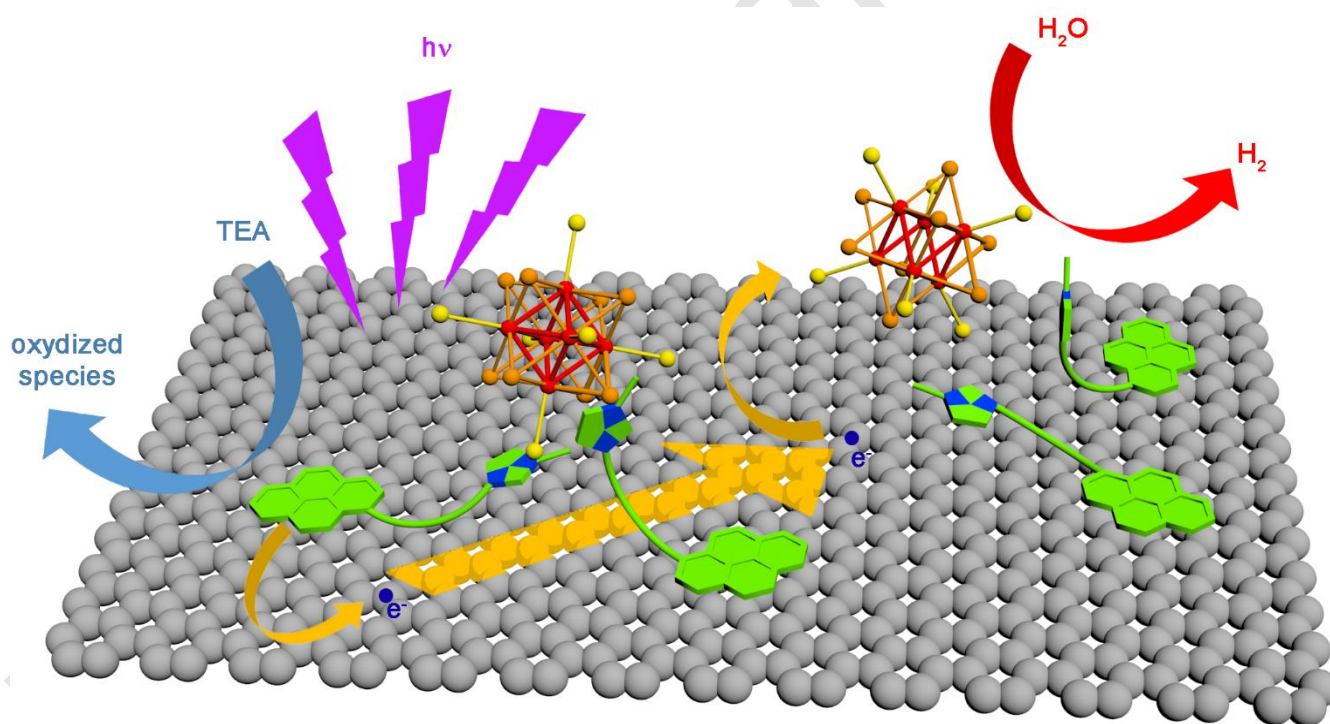


**Figure 7.** Representation of the photoexcited electron transfer and H<sub>2</sub> evolution over Py<sub>2</sub>Mo@Gene photocatalyst with the assistance of TEA under light irradiation.

## CONCLUSIONS

We show in this work that red NIR emissive octahedral transition metal clusters can be easily associated to graphene nanosheets using non-covalent interactions. To do so, organic linkers made of an imidazolium head and either a long alkyl chain or a pyrene group were specifically designed to interact with the anionic cluster and the graphene surface simultaneously. Adsorption studies demonstrated that the pyrene containing cation was the most efficient one to bind the anionic cluster onto the graphene surface. The components association was demonstrated by several techniques such as HR-TEM, EDX analyses, FT-IR and Raman spectroscopies. Photophysical studies of the **Py<sub>2</sub>Mo** hybrid complex in solution evidenced a partial energy transfer between the pyrene containing cations and the anionic cluster unit. Taking into account the low amount of pyrene triplet state produced during light excitation, we suspect that this energy transfer is more likely to involve the S<sub>1</sub>(Py) to S<sub>1</sub>(Mo) transition followed by an ISC to the T<sub>1</sub>(Mo<sub>6</sub>) state than a transfer from the T<sub>1</sub>(Py) to the T<sub>1</sub>(Mo<sub>6</sub>) states.

Once supported onto graphene, **Py<sub>2</sub>Mo** transfers its energy to the graphene surface which in turns conducts electrons to the catalytic active sites for hydrogen generation. Photocatalytic HER production in water studies have demonstrated the potential of such hybrids in the generation of hydrogen. In fact, the H<sub>2</sub> production efficiency of **Py<sub>2</sub>Mo** increases by a factor of 2.8 once grafted on graphene surface. The improvement of the H<sub>2</sub> production activity is attributed to the synergetic effect between graphene and the hybrid cluster complex, since graphene facilitates the charge separation activity and enhances the energy and electron transfer of the cluster photocatalyst. In addition, the extended aromatic lattice and, in consequence, the excellent electronic conduction of graphene sheets is preserved during the grafting of **Py<sub>2</sub>Mo**, thanks to the use of non-covalent interactions to maintain the assembly. Hence, this supramolecular strategy opens wide perspectives

in terms of research prospects to design most efficient anionic clusters/graphene hybrids for hydrogen production.

## EXPERIMENTAL SECTION

### Reagents and solvents.

Graphite, triethylamine (TEA), diethylether, methanol, acetone (ACS analytical grade), dichloromethane (Chromasolv for HPLC), and anhydrous DMF were obtained from commercial resources (Sigma-Aldrich and Scharlau). Graphene nanoplatelet aggregates (surface area  $500 \text{ m}^2 \text{ g}^{-1}$ ) were purchased from Strem. The  $\text{Cs}_2\text{Mo}_6\text{I}_8(\text{O}_2\text{CC}_2\text{F}_5)_6$  (**Cs<sub>2</sub>Mo**) precursor are prepared by following reported procedures.<sup>33</sup> The (1-methyl-3-(4-(pyren-1-yl)butyl)-1H-imidazol-3-ium bromide) **PyBr** salt has been prepared in a two-step reaction from 2-pyrenebutanol,<sup>107</sup> as described in the literature.<sup>108</sup> Dichloromethane and diethylether were dried and deoxygenated by passing these solvents through commercial columns of CuO followed by alumina under nitrogen atmosphere.

### Synthesis of the materials.

*Preparation of the **Py<sub>2</sub>Mo** complex:* to an acetone solution of **Cs<sub>2</sub>Mo**, was added a solution of **PyBr** in methanol under argon. The mixture was magnetically stirred for 48 h in the dark and then was filtered through a Celite® pad. The orange solution was then evaporated to yield a red-orange powder. <sup>1</sup>H-NMR (400 MHz, acetone-d<sub>6</sub>):  $\delta$  (ppm) = 1.96 (m, 2H, -CH<sub>2</sub>-), 1.77 (m, 2H, -CH<sub>2</sub>-), 3.81 (s, 3H, CH<sub>3</sub>-N), 4.25 (t, 2H,  $J=7.1\text{Hz}$ , -CH<sub>2</sub>-N), 7.67 (t, 1H,  $J=1.7\text{Hz}$ , -N-CH-CH-N-), 7.77 (t, 1H,  $J=1.7\text{Hz}$ , -N-CH-CH-N-), 8.36-7.95 (m, 9H, C<sub>Ar</sub>), 9.08 (s, 1H, CH, -N-CH-N-); <sup>19</sup>F-NMR (376 MHz, acetone-d<sub>6</sub>):  $\delta$  (ppm) = -83 (3F), -120 (2F); ESI-MS (CH<sub>3</sub>CN):  $m/z$ : 1284.3 [M(2-)], 339.5 [M+]



*Synthesis of 1-methyl-3-nonyl-imidazolium bromide (ImBr):* 1-N-methylimidazol (1.03gr, 12.5mmol) and 1-Bromononane (3.33g, 15 mmol) were mixed with 50 ml of CHCl<sub>3</sub>. The mixture was stirred under reflux for 15 hours. After evaporation of solvent under vacuum, the obtained colorless oil is washed three times with 50 ml of a cyclohexane:ethyl acetate mixture (1:1). The oil was recovered via a separating funnel, dried under vacuum to yield the desired compound (yield: 67%). <sup>1</sup>H-NMR (400 MHz, acetone-d<sub>6</sub>): δ (ppm) = 0.79 (t, 3H, CH<sub>3</sub>), 1.25-1.16 (m, 14H, (CH<sub>2</sub>)<sub>7</sub>), 1.84 (m, 2H, -CH<sub>2</sub>-CH<sub>2</sub>-N), 4.10 (s, 3H, CH<sub>3</sub>-N), 4.25 (t, 2H, -CH<sub>2</sub>-N), 7.45 (1H, s, -N-CH-CH-N-), 7.65 (1H, s, -N-CH-CH-N-), 10.24 (1H, s, -N-CH-N-). ESI-MS (CH<sub>3</sub>CN): 223.4 [M<sup>+</sup>].

*Preparation of the Im<sub>2</sub>Mo complex:* to an acetone solution of Cs<sub>2</sub>Mo was added a solution of ImBr in methanol under argon. The mixture was magnetically stirred for 48 h in the dark and then was filtered through a Celite® pad. The orange solution was then evaporated to yield a red-orange powder. <sup>1</sup>H-NMR (400 MHz, acetone-d<sub>6</sub>): δ (ppm) = 0.88 (t, 3H, CH<sub>3</sub>), 1.37-1.28 (m, 14H, (CH<sub>2</sub>)<sub>7</sub>), 1.98 (m, 2H, -CH<sub>2</sub>-CH<sub>2</sub>-N), 4.11 (s, 3H, CH<sub>3</sub>-N), 4.41 (t, 2H, -CH<sub>2</sub>-N), 7.77 (1H, s, -N-CH-CH-N-), 7.83 (1H, s, -N-CH-CH-N-), 9.15 (1H, s, -N-CH-N-); <sup>19</sup>F-NMR (acetone-d<sub>6</sub>): δ (ppm) = -83 (3F), -120 (2F); ESI-MS (CH<sub>3</sub>CN): m/z: 1284.3 [M(2-)]. 223.4 [M<sup>+</sup>].

*Preparation of the Py<sub>2</sub>Mo@Gene nanocomposite:* an excess of Py<sub>2</sub>Mo (22 mg, 0.007 mmol) was added to a graphene suspension (15 mg in 60 mL of dried dichloromethane) in a Schlenk flask under argon. The mixture was sonicated with an ultrasound source (400 W, Branson ultrasonic bath) for 1 h, and magnetically stirred for 24 h. The solid product was separated from the solution by filtration under vacuum, was washed several times with dichloromethane and diethylether, and dried under vacuum to provide 25 mg of a black product identified as Py<sub>2</sub>Mo@Gene nanocomposite. This material was stored in a desiccator. The amount of molybdenum present in

the sample (1.74 % w/w) has been determined by ICP analysis of the liquid phase after treatment of the solid with aqua regia. This material has been characterized by XRD, HR-TEM, STEM/EDS, IR, and Raman techniques.

## ASSOCIATED CONTENT

**Supporting Information.** Characterization techniques, detailed X-ray structural analysis of **Py<sub>2</sub>Mo**, ESI mass spectra, adsorption experiments, HR-TEM micrographs, STEM/EDS analysis of **Py<sub>2</sub>Mo@Gene**, photophysics, laser flash photolysis experiments, calculations of **Py<sub>2</sub>Mo** singlet and triplet excited state, and photocatalytic hydrogen production conditions. This material is available free of charge.

**Accession Codes.** CCDC 1866933 contains the supplementary crystallographic data for this paper. These data can be obtained free of charge via [www.ccdc.cam.ac.uk/data\\_request/cif](http://www.ccdc.cam.ac.uk/data_request/cif), or by emailing [data\\_request@ccdc.cam.ac.uk](mailto:data_request@ccdc.cam.ac.uk), or by contacting The Cambridge Crystallographic Data Centre, 12 Union Road, Cambridge CB2 1EZ, UK; fax: +44 1223 336033.

The following file is available free of charge.  
electronic supporting informations (PDF)

## AUTHOR INFORMATION

### Corresponding Author

\*mfeliz@itq.upv.es. \*yann.molard@univ-rennes1.fr.

### Author Contributions

The manuscript was written through contributions of all authors. All authors have given approval to the final version of the manuscript.

### Funding Sources

The Severo Ochoa Program (SEV-2016-0683), Ministerio de Ciencia, Innovación y Universidades (PGC2018-099744), Consejo Superior de Investigaciones Científicas (I-Link1063) and University of Rennes.

### Notes

The authors declare no competing financial interests.

### ACKNOWLEDGMENT

We would like to thank Dr. Marta Puche for her technical assistance with the preparation of dispersed graphene solutions at the ITQ.

### REFERENCES

1. Cotton, F. A., Metal Atom Clusters in Oxide Systems. *Inorg. Chem.* **1964**, 3 (9), 1217-1220.
2. Maverick, A. W.; Gray, H. B., Luminescence and Redox Photochemistry of the Molybdenum(II) Cluster  $\text{Mo}_6\text{Cl}_{14}(2-)$ . *J. Am. Chem. Soc.* **1981**, 103 (5), 1298-1300.
3. Nocera, D. G.; Gray, H. B., Electrochemical reduction of molybdenum(II) and tungsten(II) halide cluster ions. Electrogenated chemiluminescence of tetradecachlorohexamolybdate(2-) ion. *J. Am. Chem. Soc.* **1984**, 106 (3), 824-825.

4. Larina, T. V.; Ikorskii, V. N.; Vasenin, N. T.; Anufrienko, V. F.; Naumov, N. G.; Ostanina, E. V.; Fedorov, V. E., Electronic state of rhenium complexes with octahedral chalcocyanide cluster anions  $[\text{Re}(6)\text{Q}(8)(\text{CN})(6)](3-)$  ( $\text{Q}=\text{S}, \text{Se}, \text{Te}$ ). EPR and magnetic susceptibility studies. *Russ. J. Coord. Chem.* **2002**, 28 (8), 554-556.
5. Tulsy, E. G.; Crawford, N. R. M.; Baudron, S. A.; Batail, P.; Long, J. R., Cluster-to-Metal Magnetic Coupling: Synthesis and Characterization of 25-Electron  $[\text{Re}_6\text{-nOs}_n\text{Se}_8(\text{CN})_6](5\text{-n})$  ( $n = 1, 2$ ) Clusters and  $\{\text{Re}_6\text{-nOs}_n\text{Se}_8[\text{CNCu}(\text{Me}_6\text{tren})]_6\}^{9+}$  ( $n = 0, 1, 2$ ) Assemblies. *J. Am. Chem. Soc.* **2003**, 125 (50), 15543-15553.
6. Barras, A.; Cordier, S.; Boukherroub, R., Fast photocatalytic degradation of rhodamine B over  $[\text{Mo}_6\text{Br}_8(\text{N}_3)_6]^{2-}$  cluster units under sun light irradiation. *Appl. Catal., B* **2012**, 123-124, 1-8.
7. Beltran, A.; Mikhailov, M.; Sokolov, M. N.; Perez-Laguna, V.; Rezusta, A.; Revillo, M. J.; Galindo, F., A photobleaching resistant polymer supported hexanuclear molybdenum iodide cluster for photocatalytic oxygenations and photodynamic inactivation of *Staphylococcus aureus*. *J. Mater. Chem. B* **2016**, 4 (36), 5975-5979.
8. Buzek, D.; Hynek, J.; Kucerakova, M.; Kirakci, K.; Demel, J.; Lang, K.,  $\text{MoII}$  Cluster Complex-Based Coordination Polymer as an Efficient Heterogeneous Catalyst in the Suzuki-Miyaura Coupling Reaction. *Eur. J. Inorg. Chem.* **2016**, 2016 (28), 4668-4673.
9. Feliz, M.; Puche, M.; Atienzar, P.; Concepcion, P.; Cordier, S.; Molard, Y., In situ generation of active molybdenum octahedral clusters for photocatalytic hydrogen production from water and their stabilization onto graphene oxide surfaces. *ChemSusChem* **2016**, 9 (15), 1963-1971.

10. Daigre, G.; Costuas, K.; Tarasenko, M. S.; Ledneva, A. Y.; Naumov, N. G.; Lemoine, P.; Guizouarn, T.; Molard, Y.; Amela-Cortes, M.; Audebrand, N.; Cordier, S., Stabilization of Ni<sup>2+</sup> dimers in hexacyano Mo<sub>6</sub> cluster-based Prussian blue derivatives: experimental and theoretical investigations of magnetic properties. *Dalton Trans.* **2018**, 47 (4), 1122-1130.
11. Garreau, A.; Massuyeau, F.; Cordier, S.; Molard, Y.; Gautron, E.; Bertoncini, P.; Faulques, E.; Wery, J.; Humbert, B.; Bulou, A.; Duvail, J.-L., Color Control in Coaxial Two-Luminophore Nanowires. *ACS Nano* **2013**, 7 (4), 2977-2987.
12. Zhao, Y.; Lunt, R. R., Transparent Luminescent Solar Concentrators for Large-Area Solar Windows Enabled by Massive Stokes-Shift Nanocluster Phosphors. *Adv. Energy Mater.* **2013**, 3 (9), 1143-1148.
13. Amela-Cortes, M.; Garreau, A.; Cordier, S.; Faulques, E.; Duvail, J.-L.; Molard, Y., Deep red luminescent hybrid copolymer materials with high transition metal cluster content. *J. Mater. Chem. C* **2014**, 2 (8), 1545-1552.
14. Prevot, M.; Amela-Cortes, M.; Manna, S. K.; Lefort, R.; Cordier, S.; Folliot, H.; Dupont, L.; Molard, Y., Design and Integration in Electro-Optic Devices of Highly Efficient and Robust Red-NIR Phosphorescent Nematic Hybrid Liquid Crystals Containing [Mo<sub>6</sub>I<sub>8</sub>(OCOCnF<sub>2n+1</sub>)<sub>6</sub>]<sup>2-</sup> (n = 1, 2, 3) Nanoclusters. *Adv. Funct. Mater.* **2015**, 25 (31), 4966-4975.
15. Robin, M.; Kuai, W.; Amela-Cortes, M.; Cordier, S.; Molard, Y.; Mohammed-Brahim, T.; Jacques, E.; Harnois, M., Epoxy Based Ink as Versatile Material for Inkjet-Printed Devices. *ACS Appl. Mater. Interfaces* **2015**, 7 (39), 21975-21984.

16. Bignon, J.; Huby, N.; Amela-Cortes, M.; Molard, Y.; Garreau, A.; Cordier, S.; Bêche, B.; Duvail, J. L., Efficient active waveguiding properties of Mo 6 nano-cluster-doped polymer nanotubes. *Nanotechnology* **2016**, *27* (25), 255201.
17. Robin, M.; Dumait, N.; Amela-Cortes, M.; Roiland, C.; Harnois, M.; Jacques, E.; Folliot, H.; Molard, Y., Direct Integration of Red-NIR Emissive Ceramic-like  $\text{AnM}_6\text{X}_8\text{Xa}_6$  Metal Cluster Salts in Organic Copolymers Using Supramolecular Interactions. *Chem. - Eur. J.* **2018**, *24* (19), 4825-4829.
18. Krasilnikova, A. A.; Shestopalov, M. A.; Brylev, K. A.; Kirilova, I. A.; Khripko, O. P.; Zubareva, K. E.; Khripko, Y. I.; Podorognaya, V. T.; Shestopalova, L. V.; Fedorov, V. E.; Mironov, Y. V., Prospects of molybdenum and rhenium octahedral cluster complexes as X-ray contrast agents. *J. Inorg. Biochem.* **2015**, *144*, 13-17.
19. Kirakci, K.; Kubát, P.; Fejfarová, K.; Martinčík, J.; Nikl, M.; Lang, K., X-ray Inducible Luminescence and Singlet Oxygen Sensitization by an Octahedral Molybdenum Cluster Compound: A New Class of Nanoscintillators. *Inorg. Chem.* **2016**, *55* (2), 803-809.
20. Solovieva, A. O.; Kirakci, K.; Ivanov, A. A.; Kubat, P.; Pozmogova, T. N.; Miroshnichenko, S. M.; Vorontsova, E. V.; Chechushkov, A. V.; Trifonova, K. E.; Fufaeva, M. S.; Kretov, E. I.; Mironov, Y. V.; Poveschenko, A. F.; Lang, K.; Shestopalov, M. A., Singlet Oxygen Production and Biological Activity of Hexanuclear Chalcocyanide Rhenium Cluster Complexes  $[\{\text{Re}_6\text{Q}_8\}(\text{CN})_6]^{4-}$  (Q = S, Se, Te). *Inorg. Chem.* **2017**, *56* (21), 13491-13499.
21. Brandhonneur, N.; Hatahet, T.; Amela-Cortes, M.; Molard, Y.; Cordier, S.; Dollo, G., Molybdenum cluster loaded PLGA nanoparticles: An innovative theranostic approach for the treatment of ovarian cancer. *Eur. J. Pharm. Biopharm.* **2018**, *125*, 95-105.

22. Kumar, P.; Kumar, S.; Cordier, S.; Paofai, S.; Boukherroub, R.; Jain, S. L., Photoreduction of CO<sub>2</sub> to methanol with hexanuclear molybdenum [Mo<sub>6</sub>Br<sub>14</sub>]<sup>2-</sup> cluster units under visible light irradiation. *RSC Advances* **2014**, 4 (20), 10420-10423.
23. Golden, J. H.; Deng, H. B.; Disalvo, F. J.; Frechet, J. M. J.; Thompson, P. M., Monodisperse Metal-Clusters 10-Angstroms in Diameter in a Polymeric Host - the Monomer-as-Solvent Approach. *Science* **1995**, 268 (5216), 1463-1466.
24. Jackson, J. A.; Newsham, M. D.; Worsham, C.; Nocera, D. G., Efficient singlet oxygen generation from polymers derivatized with hexanuclear molybdenum clusters. *Chem. Mater.* **1996**, 8 (2), 558-564.
25. Cordier, S.; Molard, Y.; Brylev, K. A.; Mironov, Y. V.; Grasset, F.; Fabre, B.; Naumov, N. G., Advances in the Engineering of Near Infrared Emitting Liquid Crystals and Copolymers, Extended Porous Frameworks, Theranostic Tools and Molecular Junctions Using Tailored Re<sub>6</sub> Cluster Building Blocks. *J. Cluster Sci.* **2015**, 26, 53-81.
26. Cordier, S.; Grasset, F.; Molard, Y.; Amela-Cortes, M.; Boukherroub, R.; Ravaine, S.; Mortier, M.; Ohashi, N.; Saito, N.; Haneda, H., Inorganic Molybdenum Octahedral Nanosized Cluster Units, Versatile Functional Building Block for Nanoarchitectonics. *J. Inorg. Organomet. Polym. Mater.* **2015**, 25 (2), 189-204.
27. Molard, Y., Clustomesogens: Liquid Crystalline Hybrid Nanomaterials Containing Functional Metal Nanoclusters. *Acc. Chem. Res.* **2016**, 49 (8), 1514-1523.

28. Guy, K.; Ehni, P.; Paofai, S.; Forschner, R.; Roiland, C.; Amela-Cortes, M.; Cordier, S.; Laschat, S.; Molard, Y., Lord of The Crowns: A New Precious in the Kingdom of Clustomesogens. *Angew. Chem. Int. Ed.* **2018**, 57 (36), 11692-11696.
29. Sokolov, M. N.; Brylev, K. A.; Abramov, P. A.; Gallyamov, M. R.; Novozhilov, I. N.; Kitamura, N.; Mikhaylov, M. A., Complexes of  $\{W_6I_8\}^{4+}$  Clusters with Carboxylates: Preparation, Electrochemistry, and Luminescence. *Eur. J. Inorg. Chem.* **2017**, 2017 (35), 4131-4137.
30. Sokolov, M. N.; Mihailov, M. A.; Peresypkina, E. V.; Brylev, K. A.; Kitamura, N.; Fedin, V. P., Highly luminescent complexes  $[Mo_6X_8(n-C_3F_7COO)_6]^{2-}$  ( $X = Br, I$ ). *Dalton Trans.* **2011**, 40 (24), 6375-6377.
31. Kirakci, K.; Kubát, P.; Dušek, M.; Fejfarová, K.; Šícha, V.; Mosinger, J.; Lang, K., A Highly Luminescent Hexanuclear Molybdenum Cluster – A Promising Candidate toward Photoactive Materials. *Eur. J. Inorg. Chem.* **2012**, (19), 3107-3111.
32. Kirakci, K.; Kubat, P.; Langmaier, J.; Polivka, T.; Fuciman, M.; Fejfarova, K.; Lang, K., A comparative study of the redox and excited state properties of  $(nBu_4N)_2[Mo_6X_{14}]$  and  $(nBu_4N)_2[Mo_6X_8(CF_3COO)_6]$  ( $X = Cl, Br, \text{ or } I$ ). *Dalton Trans.* **2013**, 42 (19), 7224-7232.
33. Amela-Cortes, M.; Molard, Y.; Paofai, S.; Desert, A.; Duvail, J.-L.; Naumov, N. G.; Cordier, S., Versatility of the ionic assembling method to design highly luminescent PMMA nanocomposites containing  $[M_6Q_i8La_6]^{n-}$  octahedral nano-building blocks. *Dalton Trans.* **2016**, 45 (1), 237-245.



34. Mikhailov, M. A.; Brylev, K. A.; Abramov, P. A.; Sakuda, E.; Akagi, S.; Ito, A.; Kitamura, N.; Sokolov, M. N., Synthetic Tuning of Redox, Spectroscopic, and Photophysical Properties of {Mo<sub>6</sub>I<sub>8</sub>}<sup>4+</sup> Core Cluster Complexes by Terminal Carboxylate Ligands. *Inorg. Chem.* **2016**, *55* (17), 8437-8445.
35. Riehl, L.; Seyboldt, A.; Strobele, M.; Enseling, D.; Justel, T.; Westberg, M.; Ogilby, P. R.; Meyer, H. J., A ligand substituted tungsten iodide cluster: luminescence vs. singlet oxygen production. *Dalton Trans.* **2016**, *45* (39), 15500-15506.
36. Akagi, S.; Fujii, S.; Horiguchi, T.; Kitamura, N., pK<sub>a</sub>(L) Dependences of Structural, Electrochemical, and Photophysical Properties of Octahedral Hexamolybdenum(II) Clusters: [Mo<sub>6</sub>X<sub>8</sub>L<sub>6</sub>]<sup>2-</sup> (X = Br or I; L = carboxylate). *J. Cluster Sci.* **2017**, *28* (2), 757-772.
37. Kirakci, K.; Zelenka, J.; Rumlova, M.; Martincik, J.; Nikl, M.; Ruml, T.; Lang, K., Octahedral molybdenum clusters as radiosensitizers for X-ray induced photodynamic therapy. *J. Mater. Chem. B* **2018**, *6* (26), 4301-4307.
38. Amela-Cortes, M.; Paofai, S.; Cordier, S.; Folliot, H.; Molard, Y., Tuned Red NIR phosphorescence of polyurethane hybrid composites embedding metallic nanoclusters for oxygen sensing. *Chem. Commun.* **2015**, *51*, 8177-8180.
39. Kudo, A.; Miseki, Y., Heterogeneous photocatalyst materials for water splitting. *Chem. Soc. Rev.* **2009**, *38* (1), 253-278.
40. Walter, M. G.; Warren, E. L.; McKone, J. R.; Boettcher, S. W.; Mi, Q.; Santori, E. A.; Lewis, N. S., Solar Water Splitting Cells. *Chem. Rev.* **2010**, *110* (11), 6446-6473.

41. Maeda, K., Photocatalytic water splitting using semiconductor particles: History and recent developments. *J. Photochem. Photobiol., C* **2011**, *12* (4), 237-268.
42. Zou, X.; Zhang, Y., Noble metal-free hydrogen evolution catalysts for water splitting. *Chem. Soc. Rev.* **2015**, *44* (15), 5148-5180.
43. Watanabe, M., Dye-sensitized photocatalyst for effective water splitting catalyst. *Sci. Technol. Adv. Mater.* **2017**, *18* (1), 705-723.
44. Zheng, D.; Pang, X.; Wang, M.; He, Y.; Lin, C.; Lin, Z., Unconventional Route to Hairy Plasmonic/Semiconductor Core/Shell Nanoparticles with Precisely Controlled Dimensions and Their Use in Solar Energy Conversion. *Chem. Mater.* **2015**, *27* (15), 5271-5278.
45. Wang, M.; Pang, X.; Zheng, D.; He, Y.; Sun, L.; Lin, C.; Lin, Z., Nonepitaxial growth of uniform and precisely size-tunable core/shell nanoparticles and their enhanced plasmon-driven photocatalysis. *J. Mater. Chem. A* **2016**, *4* (19), 7190-7199.
46. Wang, M.; Ye, M.; Iocozzia, J.; Lin, C.; Lin, Z., Plasmon-Mediated Solar Energy Conversion via Photocatalysis in Noble Metal/Semiconductor Composites. *Adv. Science* **2016**, *3* (6), 1600024.
47. Yang, J.; Fu, H.; Yang, D.; Gao, W.; Cong, R.; Yang, T.,  $\text{ZnGa}_{2-x}\text{In}_x\text{S}_4$  ( $0 \leq x \leq 0.4$ ) and  $\text{Zn}_{1-2y}(\text{CuGa})_y\text{Ga}_{1.7}\text{In}_{0.3}\text{S}_4$  ( $0.1 \leq y \leq 0.2$ ): Optimize Visible Light Photocatalytic  $\text{H}_2$  Evolution by Fine Modulation of Band Structures. *Inorg. Chem.* **2015**, *54* (5), 2467-2473.
48. Yu, W.; Zhang, S.; Chen, J.; Xia, P.; Richter, M. H.; Chen, L.; Xu, W.; Jin, J.; Chen, S.; Peng, T., Biomimetic Z-scheme photocatalyst with a tandem solid-state electron flow catalyzing  $\text{H}_2$  evolution. *J. Mater. Chem. A* **2018**, *6* (32), 15668-15674.

49. Hao, Q.; Song, Y.; Ji, H.; Mo, Z.; She, X.; Deng, J.; Muhmood, T.; Wu, X.; Yuan, S.; Xu, H.; Li, H., Surface N modified 2D g-C<sub>3</sub>N<sub>4</sub> nanosheets derived from DMF for photocatalytic H<sub>2</sub> evolution. *Appl. Surf. Sci.* **2018**, *459*, 845-852.
50. Xia, Y.; Cheng, B.; Fan, J.; Yu, J.; Liu, G., Unraveling Photoexcited Charge Transfer Pathway and Process of CdS/Graphene Nanoribbon Composites toward Visible-Light Photocatalytic Hydrogen Evolution. *Small* **2019**, *15* (34), 1902459.
51. Chang, C.-J.; Lin, Y.-G.; Weng, H.-T.; Wei, Y.-H., Photocatalytic hydrogen production from glycerol solution at room temperature by ZnO-ZnS/graphene photocatalysts. *Appl. Surf. Sci.* **2018**, *451*, 198-206.
52. Xu, D.; Li, L.; He, R.; Qi, L.; Zhang, L.; Cheng, B., Noble metal-free RGO/TiO<sub>2</sub> composite nanofiber with enhanced photocatalytic H<sub>2</sub>-production performance. *Appl. Surf. Sci.* **2018**, *434*, 620-625.
53. Osterloh, F. E., Inorganic Materials as Catalysts for Photochemical Splitting of Water. *Chem. Mater.* **2008**, *20* (1), 35-54.
54. Sun, Y.; Wu, Q.; Shi, G., Graphene based new energy materials. *Energy Environ. Sci.* **2011**, *4* (4), 1113-1132.
55. Wang, J.; Cui, W.; Liu, Q.; Xing, Z.; Asiri, A. M.; Sun, X., Recent Progress in Cobalt-Based Heterogeneous Catalysts for Electrochemical Water Splitting. *Adv. Mater.* **2016**, *28* (2), 215-230.
56. Kamat, P. V., Graphene-Based Nanoassemblies for Energy Conversion. *J. Phys. Chem. Lett.* **2011**, *2* (3), 242-251.

57. Han, L.; Wang, P.; Dong, S., Progress in graphene-based photoactive nanocomposites as a promising class of photocatalyst. *Nanoscale* **2012**, 4 (19), 5814-5825.
58. Xiang, Q.; Yu, J., Graphene-Based Photocatalysts for Hydrogen Generation. *J. Phys. Chem. Lett.* **2013**, 4 (5), 753-759.
59. Huo, J.; Zhang, Y.-B.; Zou, W.-Y.; Hu, X.; Deng, Q.; Chen, D., Mini-review on an engineering approach towards the selection of transition metal complex-based catalysts for photocatalytic H<sub>2</sub> production. *Catal. Sci. Technol.* **2019**, 9 (11), 2716-2727.
60. Attia, Y.; Samer, M., Metal clusters: New era of hydrogen production. *Renew. Sust. Energy Rev.* **2017**, 79, 878-892.
61. Peiris, S.; McMurtrie, J.; Zhu, H.-Y., Metal nanoparticle photocatalysts: emerging processes for green organic synthesis. *Catal. Sci. Technol.* **2016**, 6 (2), 320-338.
62. Kim, H.-i.; Moon, G.-h.; Monllor-Satoca, D.; Park, Y.; Choi, W., Solar Photoconversion Using Graphene/TiO<sub>2</sub> Composites: Nanographene Shell on TiO<sub>2</sub> Core versus TiO<sub>2</sub> Nanoparticles on Graphene Sheet. *J. Phys. Chem. C* **2012**, 116 (1), 1535-1543.
63. Chang, K.; Mei, Z.; Wang, T.; Kang, Q.; Ouyang, S.; Ye, J., MoS<sub>2</sub>/Graphene Cocatalyst for Efficient Photocatalytic H<sub>2</sub> Evolution under Visible Light Irradiation. *ACS Nano* **2014**, 8 (7), 7078-7087.
64. Li, H.; Yu, K.; Li, C.; Tang, Z.; Guo, B.; Lei, X.; Fu, H.; Zhu, Z., Charge-Transfer Induced High Efficient Hydrogen Evolution of MoS<sub>2</sub>/graphene Cocatalyst. *Scientific Reports* **2015**, 5, 18730.

65. Georgakilas, V.; Tiwari, J. N.; Kemp, K. C.; Perman, J. A.; Bourlinos, A. B.; Kim, K. S.; Zboril, R., Noncovalent Functionalization of Graphene and Graphene Oxide for Energy Materials, Biosensing, Catalytic, and Biomedical Applications. *Chem. Rev.* **2016**, *116* (9), 5464-5519.
66. Li, X.; Yu, J.; Wageh, S.; Al-Ghamdi, A. A.; Xie, J., Graphene in Photocatalysis: A Review. *Small* **2016**, *12* (48), 6640-6696.
67. Fabre, B.; Cordier, S.; Molard, Y.; Perrin, C.; Ababou-Girard, S.; Godet, C., Electrochemical and Charge Transport Behavior of Molybdenum-Based Metallic Cluster Layers Immobilized on Modified n- and p-Type Si(111) Surfaces. *J. Phys. Chem. C* **2009**, *113* (40), 17437-17446.
68. Godet, C.; Ababou-Girard, S.; Fabre, B.; Molard, Y.; Fadjie-Djomkam, A. B.; Deputier, S.; Guilloux-Viry, M.; Cordier, S., Surface immobilization of Mo<sub>6</sub>I<sub>8</sub> octahedral cluster cores on functionalized amorphous carbon using a pyridine complexation strategy. *Diamond Relat. Mater.* **2015**, *55*, 131-138.
69. Cordier, S.; Fabre, B.; Molard, Y.; Fadjie-Djomkam, A.-B.; Turban, P.; Tricot, S.; Ababou-Girard, S.; Godet, C., Elaboration, Characterizations, and Energetics of Robust Mo<sub>6</sub> Cluster-Terminated Silicon-Bound Molecular Junctions. *J. Phys. Chem. C* **2016**, *120* (4), 2324-2334.
70. Wang, H.; Ma, K.; Xu, B.; Tian, W., Tunable Supramolecular Interactions of Aggregation-Induced Emission Probe and Graphene Oxide with Biomolecules: An Approach toward Ultrasensitive Label-Free and “Turn-On” DNA Sensing. *Small* **2016**, *12* (47), 6613-6622.

71. Sabater, S.; Mata, J. A.; Peris, E., Immobilization of Pyrene-Tagged Palladium and Ruthenium Complexes onto Reduced Graphene Oxide: An Efficient and Highly Recyclable Catalyst for Hydrodefluorination. *Organomet.* **2015**, *34* (7), 1186-1190.
72. Zhang, X.; Huisman, E. H.; Gurram, M.; Browne, W. R.; van Wees, B. J.; Feringa, B. L., Supramolecular Chemistry on Graphene Field-Effect Transistors. *Small* **2014**, *10* (9), 1735-1740.
73. Zhou, X.; Wu, T.; Ding, K.; Hu, B.; Hou, M.; Han, B., Dispersion of graphene sheets in ionic liquid [bmim][PF<sub>6</sub>] stabilized by an ionic liquid polymer. *Chem. Commun.* **2010**, *46* (3), 386-388.
74. Wang, J.; Chen, Z.; Chen, B., Adsorption of Polycyclic Aromatic Hydrocarbons by Graphene and Graphene Oxide Nanosheets. *Environ. Sci. Technol.* **2014**, *48* (9), 4817-4825.
75. Shakourian-Fard, M.; Jamshidi, Z.; Bayat, A.; Kamath, G., Meta-Hybrid Density Functional Theory Study of Adsorption of Imidazolium- and Ammonium-Based Ionic Liquids on Graphene Sheet. *J. Phys. Chem. C* **2015**, *119* (13), 7095-7108.
76. Srinivasan, S.; Shin, W. H.; Choi, J. W.; Coskun, A., A bifunctional approach for the preparation of graphene and ionic liquid-based hybrid gels. *J. Mater. Chem. A* **2013**, *1* (1), 43-48.
77. Kirakci, K.; Fejfarova, K.; Kucerakova, M.; Lang, K., Hexamolybdenum Cluster Complexes with Pyrene and Anthracene Carboxylates: Ultrabright Red Emitters with the Antenna Effect. *Eur. J. Inorg. Chem.* **2014**, *14*, 2331-2336.
78. Preetz, W.; Bublit, D.; Von Schnering, H. G.; Saßmannshausen, J., Darstellung, Kristallstruktur und spektroskopische Eigenschaften der Clusteranionen [(Mo<sub>6</sub>Br<sub>8</sub>i)X<sub>6</sub>a]<sup>2-</sup> mit X<sub>a</sub> = F, Cl, Br, I. *Z. Anorg. Allg. Chem.* **1994**, *620* (2), 234-246.

79. Schoonover, J. R.; Zietlow, T. C.; Clark, D. L.; Heppert, J. A.; Chisholm, M. H.; Gray, H. B.; Sattelberger, A. P.; Woodruff, W. H., Resonance Raman Spectra of  $[M_6X_8Y_6]^{2-}$  Cluster Complexes ( $M = Mo, W$ ;  $X, Y = Cl, Br, I$ ). *Inorg. Chem.* **1996**, *35* (22), 6606-6613.
80. Ferrari, A. C., Raman spectroscopy of graphene and graphite: Disorder, electron-phonon coupling, doping and nonadiabatic effects. *Solid State Commun.* **2007**, *143* (1), 47-57.
81. Asher, S. A., Ultraviolet resonance Raman spectrometry for detection and speciation of trace polycyclic aromatic hydrocarbons. *Anal. Chem.* **1984**, *56* (4), 720-724.
82. Rumelfanger, R.; Asher, S. A.; Perry, M. B., UV Resonance Raman Characterization of Polycyclic Aromatic Hydrocarbons in Coal Liquid Distillates. *Appl. Spectro.* **1988**, *42* (2), 267-272.
83. Larsen, J.; Puntoriero, F.; Pascher, T.; McClenaghan, N.; Campagna, S.; Åkesson, E.; Sundström, V., Extending the Light-Harvesting Properties of Transition-Metal Dendrimers. *ChemPhysChem* **2007**, *8* (18), 2643-2651.
84. Amelia, M.; Lavie-Cambot, A.; McClenaghan, N. D.; Credi, A., A ratiometric luminescent oxygen sensor based on a chemically functionalized quantum dot. *Chem. Commun.* **2011**, *47* (1), 325-327.
85. Ramirez-Tagle, R.; Arratia-Pérez, R., Electronic structure and molecular properties of the  $[Mo_6X_8L_6]^{2-}$ ;  $X = Cl, Br, I$ ;  $L = F, Cl, Br, I$  clusters. *Chem. Phys. Lett.* **2008**, *460* (4-6), 438-441.
86. Costuas, K.; Garreau, A.; Bulou, A.; Fontaine, B.; Cuny, J.; Gautier, R.; Mortier, M.; Molard, Y.; Duvail, J. L.; Faulques, E.; Cordier, S., Combined theoretical and time-resolved

photoluminescence investigations of [Mo<sub>6</sub>Bri<sub>8</sub>Bra<sub>6</sub>]<sup>2-</sup> metal cluster units: evidence of dual emission. *Phys. Chem. Chem. Phys.* **2015**, *17* (43), 28574-28585.

87. Karpovich, D. S.; Blanchard, G. J., Relating the polarity-dependent fluorescence response of pyrene to vibronic coupling. Achieving a fundamental understanding of the py polarity scale. *J. Phys. Chem.* **1995**, *99* (12), 3951-3958.

88. Camerel, F.; Kinloch, F.; Jeannin, o.; Robin, M.; nayak, s. K.; Jacques, E.; Brylev, K.; Naumov, N. G.; Molard, Y., Ionic Columnar Clustomesogens: Associations between Anionic Hexanuclear Rhenium Clusters and Liquid Crystalline Triphenylene Tethered Imidazoliums. *Dalton Trans.* **2018**, *47*, 10884-10896.

89. Vining, W. J.; Caspar, J. V.; Meyer, T. J., The influence of environmental effects on excited-state lifetimes. The effect of ion pairing on metal-to-ligand charge transfer excited states. *J. Phys. Chem.* **1985**, *89* (7), 1095-1099.

90. Divya, K. P.; Savithri, S.; Ajayaghosh, A., A fluorescent molecular probe for the identification of zinc and cadmium salts by excited state charge transfer modulation. *Chem. Commun.* **2014**, *50* (45), 6020-6022.

91. Ma, Y.; Liu, S.; Yang, H.; Zeng, Y.; She, P.; Zhu, N.; Ho, C.-L.; Zhao, Q.; Huang, W.; Wong, W.-Y., Luminescence Color Tuning by Regulating Electrostatic Interaction in Light-Emitting Devices and Two-Photon Excited Information Decryption. *Inorg. Chem.* **2017**, *56* (5), 2409-2416.



92. Ma, Y.; She, P.; Zhang, K. Y.; Yang, H.; Qin, Y.; Xu, Z.; Liu, S.; Zhao, Q.; Huang, W., Dynamic metal-ligand coordination for multicolour and water-jet rewritable paper. *Nature Commun.* **2018**, *9* (1), 3.
93. Pankasem, S.; Thomas, J. K., Reflectance spectroscopic studies of the cation radical and the triplet of pyrene on alumina. *J. Phys. Chem.* **1991**, *95* (18), 6990-6996.
94. Pina, J.; Pinheiro, D.; Nascimento, B.; Pineiro, M.; Seixas de Melo, J. S., The effect of polyaromatic hydrocarbons on the spectral and photophysical properties of diaryl-pyrrole derivatives: an experimental and theoretical study. *Phys. Chem. Chem. Phys.* **2014**, *16* (34), 18319-18326.
95. Takahashi, T.; Shizu, K.; Takuma, Y.; Togashi, K.; Adachi, C., Donor-acceptor-structured 1,4-diazatriphenylene derivatives exhibiting thermally activated delayed fluorescence: design and synthesis, photophysical properties and OLED characteristics. *Sci. Tech. Adv. Mater.* **2014**, *15*, 10.
96. Kurata, R.; Tanaka, K.; Ito, A., Isolation and Characterization of Persistent Radical Cation and Dication of 2,7-Bis(dianisylamino)pyrene. *J. Org. Chem.* **2016**, *81* (1), 137-145.
97. Cao, L.; Meziani, M. J.; Sahu, S.; Sun, Y.-P., Photoluminescence Properties of Graphene versus Other Carbon Nanomaterials. *Acc. Chem. Res.* **2013**, *46* (1), 171-180.
98. Economopoulos, S. P.; Tagmatarchis, N., Multichromophores Onto Graphene: Supramolecular Non-Covalent Approaches for Efficient Light Harvesting. *J. Phys. Chem. C* **2015**, *119* (15), 8046-8053.

99. de Miguel, M.; Álvaro, M.; García, H., Graphene as a Quencher of Electronic Excited States of Photochemical Probes. *Langmuir* **2012**, *28* (5), 2849-2857.
100. Atienzar, P.; Primo, A.; Lavorato, C.; Molinari, R.; García, H., Preparation of Graphene Quantum Dots from Pyrolyzed Alginate. *Langmuir* **2013**, *29* (20), 6141-6146.
101. Min, S.; Lu, G., Sites for High Efficient Photocatalytic Hydrogen Evolution on a Limited-Layered MoS<sub>2</sub> Cocatalyst Confined on Graphene Sheets—The Role of Graphene. *J. Phys. Chem. C* **2012**, *116* (48), 25415-25424.
102. Liu, M.; Li, F.; Sun, Z.; Ma, L.; Xu, L.; Wang, Y., Noble-metal-free photocatalysts MoS<sub>2</sub>-graphene/CdS mixed nanoparticles/nanorods morphology with high visible light efficiency for H<sub>2</sub> evolution. *Chem. Commun.* **2014**, *50* (75), 11004-11007.
103. Latorre-Sánchez, M.; Esteve-Adell, I.; Primo, A.; García, H., Innovative preparation of MoS<sub>2</sub>-graphene heterostructures based on alginate containing (NH<sub>4</sub>)<sub>2</sub>MoS<sub>4</sub> and their photocatalytic activity for H<sub>2</sub> generation. *Carbon* **2015**, *81*, 587-596.
104. Meng, F.; Li, J.; Cushing, S. K.; Zhi, M.; Wu, N., Solar Hydrogen Generation by Nanoscale p-n Junction of p-type Molybdenum Disulfide/n-type Nitrogen-Doped Reduced Graphene Oxide. *J. Am. Chem. Soc.* **2013**, *135* (28), 10286-10289.
105. Matsumoto, Y.; Koinuma, M.; Ida, S.; Hayami, S.; Taniguchi, T.; Hatakeyama, K.; Tateishi, H.; Watanabe, Y.; Amano, S., Photoreaction of Graphene Oxide Nanosheets in Water. *J. Phys. Chem. C* **2011**, *115* (39), 19280-19286.
106. Xie, G.; Zhang, K.; Guo, B.; Liu, Q.; Fang, L.; Gong, J. R., Graphene-Based Materials for Hydrogen Generation from Light-Driven Water Splitting. *Adv. Mater.* **2013**, *25* (28), 3820-3839.

107. Furuta, K.; Tomokiyo, K.; Kuo, M. T.; Ishikawa, T.; Suzuki, M., Molecular design of glutathione-derived biochemical probes targeting the GS-X pump. *Tetrahedron* **1999**, 55 (24), 7529-7540.

108. Wittmann, S.; Schätz, A.; Grass, R. N.; Stark, W. J.; Reiser, O., A Recyclable Nanoparticle-Supported Palladium Catalyst for the Hydroxycarbonylation of Aryl Halides in Water. *Angew. Chem. Int. Ed.* **2010**, 49 (10), 1867-1870.

Octahedral molybdenum clusters are red NIR phosphorescent emitters.  $[\text{Mo}_6\text{I}_8(\text{OCOC}_2\text{F}_5)_6]^{2-}$  is one of the most emissive metal cluster, but demonstrates a low photocatalytic  $\text{H}_2$  production from water splitting. Its anchoring onto graphene using pyrene containing organic cations as supramolecular linkers, enhances the photocatalytic activity of the nanocomposite by 280 %.

